Research Square

Preprints are preliminary reports that have not undergone peer review.
They should not be considered conclusive, used to inform clinical practice,
or referenced by the media as validated information.

Novel graphical method for the designing of telescopes

FLORIAN BIENERT

Florian.Bienert@ifsw.uni-stuttgart.de

University of Stuttgart

Research Article

Keywords:

Posted Date: November 3rd, 2026

DOI: https://doi.org/10.21203/rs.3.rs-11332583/v1

License: This work is licensed under a Creative Commons Attribution 4.0 International License.
Read Full License

Additional Declarations: No competing interests reported.

Novel graphical method for the designing of telescopes

FLORIAN BIENERT

Universität Stuttgart, Institut for Strahlwerkzeuge (IFSW), Pfaffenwaldring 43, 70569 Stuttgart, Germany
**Corresponding author: Florian.Bienert@ifsw.uni-stuttgart.de*

Abstract: A new way to visualize telescopes for laser beams is presented. Using this novel representation in the complex plane with the already common q-parameter both understanding and designing of telescopes becomes much simpler. This publication incorporates extensive mathematical proofs that the novel representation is correct and based on that a map is derived that even allows the designing of telescopes as a quick back-of the envelope tasks during lab-work. Finally, three telescopes are designed as an example to show how the map works.

1. Introduction

The designing of telescopes typically relies on commercial software such as Zemax [1,2], BeamXpert [3], reZonator, or similar tools [4]. Although such tools are clearly capable for designing even the most complex telescopes, especially for astronomy [5–7], when designing telescopes (also called beam expanders) for lasers [2,8], however, such software can be unnecessarily complex. At the same time, purely geometric ray-optics approaches are often not sufficiently accurate for the designing of telescopes because they generally do not account for diffraction effects [9]. In addition to this, both highly advanced and less advanced software merely support intuitive understanding how beams interact with lenses and free-space propagation.

In general, in cases where a humans want to keep an overview over various design choices it is often advantageous to work with a map. This holds across many disciplines. In electronics, the Smith chart is used, in thermodynamics, the temperature–entropy (T-s) diagram, in materials science, the iron–carbon phase diagram. In optics, for example, the Ewald construction can be used to determine diffraction orders [10], the g_1-g_2 diagram is used for assessing resonator stability [11] and a $\Lambda - \theta_{\mathrm{inc}}$ map can be used for the designing of pulse compressors [12].

For the designing of telescopes already 1964 a map-based approach was proposed. The so-called gaussian beam chart, or, Collins-diagram has high similarities with the Smith-chart and enables the depiction of refraction and free-space propagation in a con-focal map [13,14]. The usage however is not straight forwards, as the implementation of a beam into the chart already needs some calculation. An additional logarithmic version was introduced by Seifert in 1968 [15]. Other graphical method were the yα-diagram and the yȳ-diagram [16,17] were beams were displayed by diagonal lines and the distance to the origin described the beam diameter.

Within this publication a much simpler usage is pursued. Therefore, an already common description of the propagation of laser beams is used: the q-parameter [18–22] which can also be combined with the classical ABCD-matrix formalism [23]. Here every Gaussian beam can be represented by its complex q-parameter, which contains the distance from the focus, z, and the Rayleigh length, z_R, as follows:

$$q = z + iz_R \tag{1}$$

Using this already widely used approach, this paper aims to present a novel way to view how laser beams behave when interacting with lenses and during free-space propagation. Based on this novel way a graphical method for the designing of telescopes is derived. This method even allows for back-of-the-envelope designing of telescopes in the lab and may enhance the understanding of how laser beams propagate even for senior scientists. First, section 2 describes how free-space propagation changes the q-parameter and section 3 explains how refraction by a thin lens changes the q-parameter. After that Section 4 summarizes the basic graphical rules that need to be applied to the q-parameter for propagation and refraction, and Section 5 presents a map that enables straightforward telescope design. Finally, Section 6 demonstrates how the map can be used within three practical design examples.

2. Propagation in free space

Consider a laser beam with the initial q-parameter q_1,

$$q_1 = z_1 + iz_{R,1} \tag{2}$$

After propagation over a distance L, the new q-parameter is given by

$$q_2 = \frac{A \cdot q_1 + B}{C \cdot q_1 + D} \tag{3}$$

with

$$M_{Prop} = \begin{bmatrix} A & B \\ C & D \end{bmatrix} = \begin{bmatrix} 1 & L \\ 0 & 1 \end{bmatrix}. \tag{4}$$

From Eqn. (2) to Eqn. (4) q_2 follows as

$$q_2 = \frac{q_1 + L}{1} = L + z_1 + iz_{R,1} \tag{5}$$

When viewing both q_1 and q_2 in the complex q-plane, this transformation corresponds to a horizontal shift, as illustrated in Fig. 1. The point representing q_1 is moved to the right by the distance L. This simple rule applies to any q-parameter during free-space propagation.

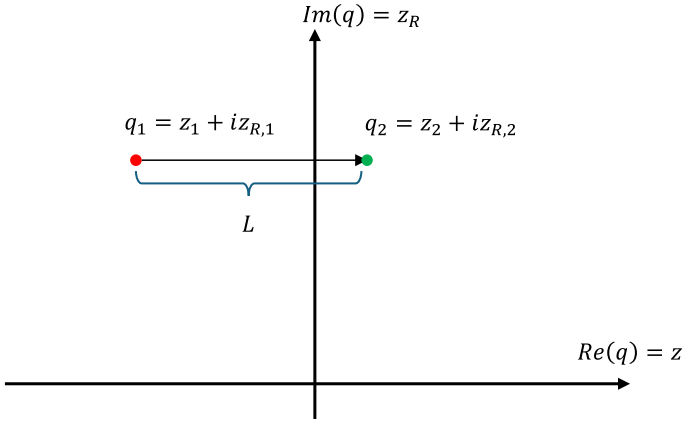


Fig. 1. Illustration of how a q-parameter changes when a simple propagation is applied. An initial q-parameter q_1 is horizontally shifted to the right by distance L.

3. Refraction by a thin lens

When a beam described by the q-parameter q_1 passes through a lens, the transformation is more complex. The new q-parameter is calculated as

$$q_2 = \frac{A \cdot q_1 + B}{C \cdot q_1 + D} \tag{6}$$

with the ABCD matrix of a thin lens given by

$$M_{Lens} = \begin{bmatrix} A & B \\ C & D \end{bmatrix} = \begin{bmatrix} 1 & 0 \\ C & 1 \end{bmatrix} = \begin{bmatrix} 1 & 0 \\ -1/f & 1 \end{bmatrix} \tag{7}$$

this yields

$$q_2 = \frac{q_1}{Cq_1 + 1}. \tag{8}$$

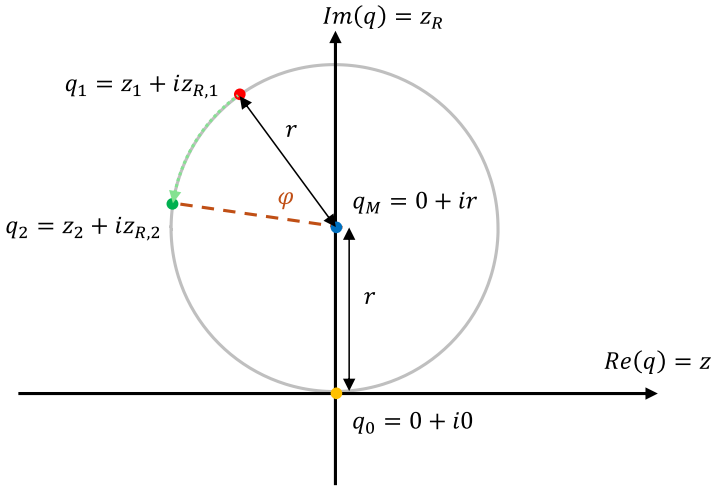


Fig. 2. Illustration of how the q-parameter of a beam changes when the beam is refracted by a lens. The original q-parameter q_1 (before the lens) is mathematically rotated around a point q_M by an angle φ. The point q_M is located on the vertical axis (with z = 0) which has the same distance to q_1 and q_0. The angle φ depends both on the q-parameter q_1 and the focal length of the lens.

Using the graphical representation in the complex plane, the transformed parameter appears as q_2, see Fig. 2. Although q_2 generally does not have the same z or z_R value as q_1, it still follows a well-defined geometrical rule: q_2 lies on the circle defined by q_0, q_M, and q_1. Here, q_0 denotes the origin of the diagram, q_1 is the initial point, and

q_M is the point located on the vertical axis (with z = 0) which has the same distance to q_1 and q_0. This means, that for any q_1 that is transformed by a lens, first a temporary circle is constructed in the complex q-plane. This circle passes through both q_0 and q_1, and its centre q_M lies on the imaginary axis. Refraction by the lens then corresponds to a rotation of q_1 around q_M by an angle φ, resulting in the new point q_2.

The proof of this behaviour is provided in Appendix A. It shows that q_2 always lies on the circumference of this circle, independent of C and therefore independent of the focal length f of the lens. The focal length only determines how far q_2 moves along the circumference. A second proof, presented in Appendix B, shows that the rotation angle φ of the q-parameter around q_M is given by

$$\varphi = -2\arctan\left(\frac{z_{R,1}}{C^{-1}+z_1}\right) = -2\arctan\left(\frac{z_{R,1}}{z_1 - f}\right). \tag{9}$$

From this proof it also follows that refracting a beam with a positive lens rotates the q-parameter in the counterclockwise direction, whereas refracting a beam with a negative lens moves it in the clockwise direction.

In addition to this, the same circle can be interpreted as an iso-line of constant beam diameter. This can also be understood intuitively, because the beam diameter immediately before and after a thin lens is unchanged. For this reason, the corresponding proof is not included here.

4. Basic rules of q moving in the complex plane

Fig. 3 applies the graphical rules derived above to a beam propagating through two lenses. Fig. 3(a) schematically shows the optical layout, while Fig. 3(b) shows the corresponding trajectory of the q-parameter in the complex plane. Initially, the beam is described by q_1 and propagates over a distance L_1 before reaching the first lens, where it is described by q_2. Since the beam is slightly convergent, q_1 is located on the left-hand side of the diagram. Free-space propagation over L_1 shifts the q-parameter horizontally to q_2. Refraction by the first, positive lens then focuses the beam and corresponds to a motion along the circle defined by q_0 and q_2 until q_3 is reached. The beam subsequently propagates over a distance L_2 to the second lens. This lens has negative optical power and therefore causes a clockwise movement along the second circle until q_5 is reached. After the second lens, the beam propagates over a further distance L_3 and finally reaches q_6. The circles also serve as iso-diameter lines, which makes it possible to estimate the beam diameter at different positions along the propagation path.

This example illustrates that the graphical method is straightforward to use while also providing additional physical insight. At any point, the degree of collimation can be estimated from the imaginary part of q, corresponding to the vertical position in the diagram. The graph also immediately indicates whether the beam is convergent or divergent and how far it is from its focus by the horizontal position in the diagram. By adding iso-diameter circles, as will be done in the next section, the evolution of the beam diameter can be accurately traced along the entire optical path. Also the total propagation distance can be obtained simply by adding up the horizontal shifts in the map.

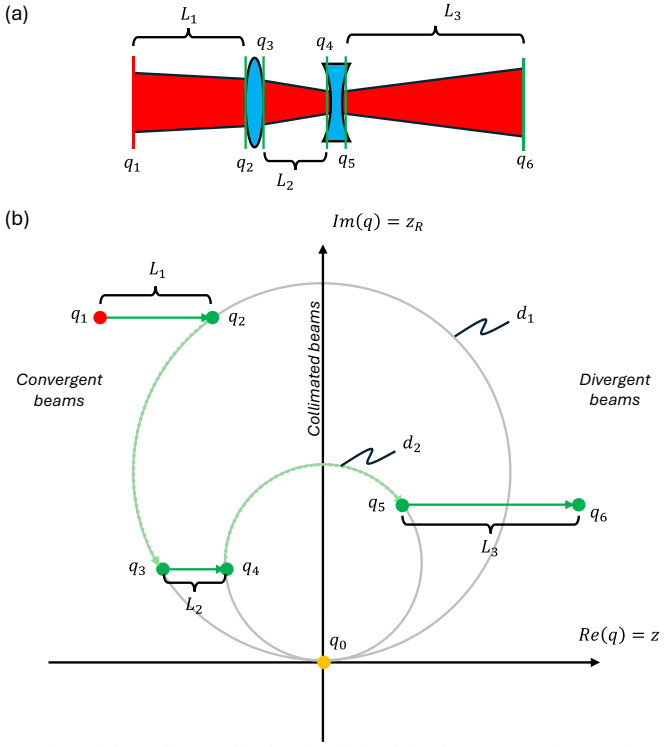


Fig. 3. Qualitative illustration of how the graphical rules derived in the two previous sections apply to a given propagation of a beam through two lenses. (a): Schematical representation of the caustic of a beam propagating through two lenses. (b): Corresponding movement of the q-parameters within the complex plane.

5. Pre-defined map

Based on the previous learnings, the map shown in Fig. 4(a) was created. It was calculated for a beam with a wavelength of $\lambda = 1030$ nm. Again, the negative part of the vertical axis of the complex diagram is not shown as it is nonphysical. Already by default the complex map shows multiple circles (magenta) with beam diameters ranging from 0 mm to 2 mm spaced by 0.1 mm. The finer lines represent increment of 0.001 mm. In addition to the magenta-colored rings, the map also contains blue lines diverging from the center. These lines represent ticks for equal dioptric steps along the circles. The thick lines are spaced by 100 mdtp while the fine lines are spaced by 10 mdtp. This means when focusing a beam through a lens having 300 mdtp, three ticks need to be passed along the circle. At the top of the map a reminder is added showing that exactly along the imaginary axis all beams are perfectly collimated while they are converging on the left (for negative z) and diverging on the right (for positive z). Also, as a reminder, it is shown how a positive and a negative lens rotate the q-parameter within the map.

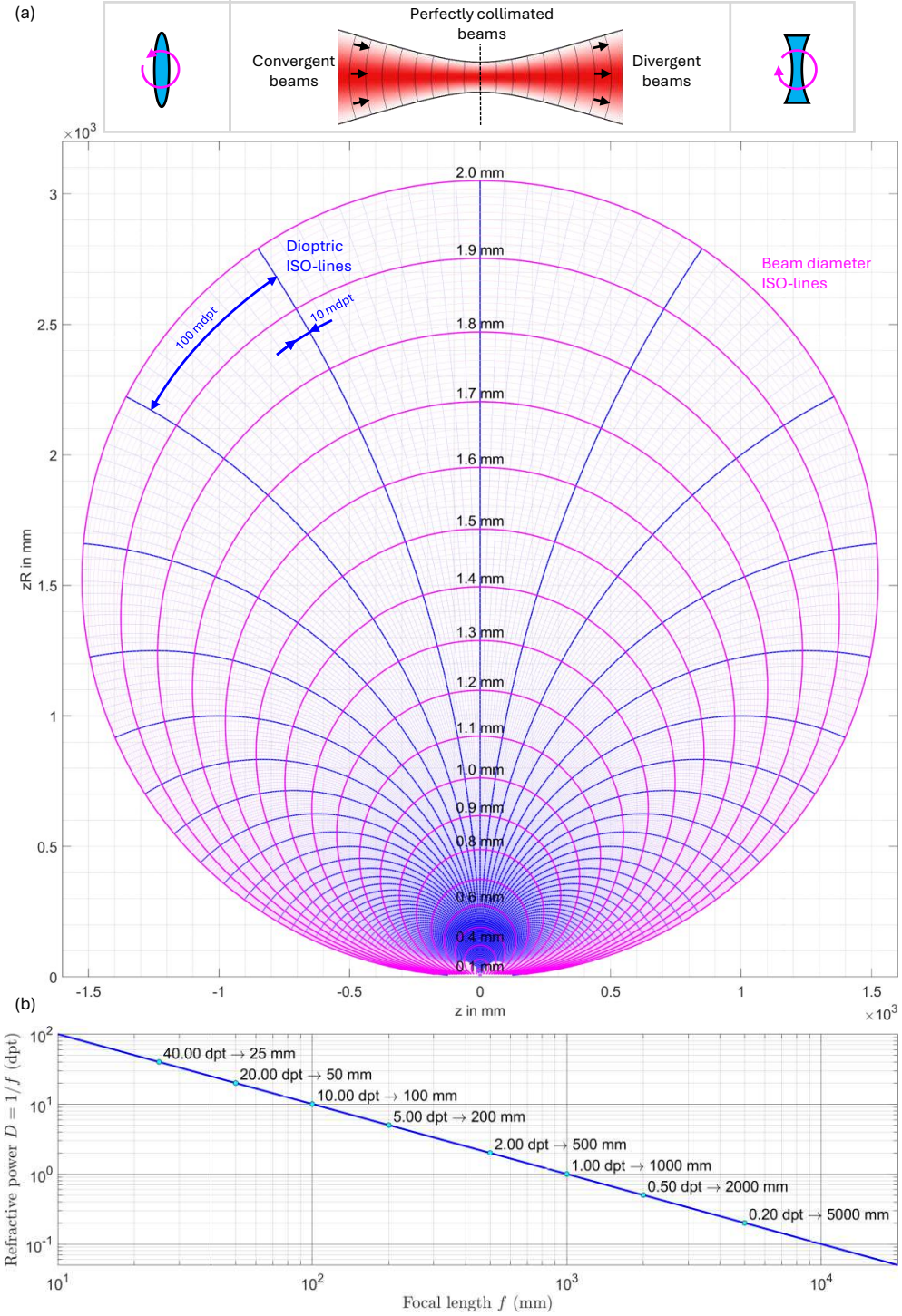


Fig. 4. Pre-defined map for a beam with $\lambda = 1030$ nm that was calculated based on the derivations from section 2 and section 3. (a): Complex plane where the q-parameters can be drawn into. The predefined rings and dioptric lines allow for simple geometrical tracing without calculations. (b): The graph helps in the transfer from focal length of a lens to its dioptric power that is used in the map.

6. Using the pre-defined map in telescope designing

Fig. 5 illustrates how the map can be used to design a telescope. Suppose that an input beam described by q_{Start} must be transformed into an output beam described by q_{End}. In the example considered here, the corresponding q-parameters are indicated in the map.

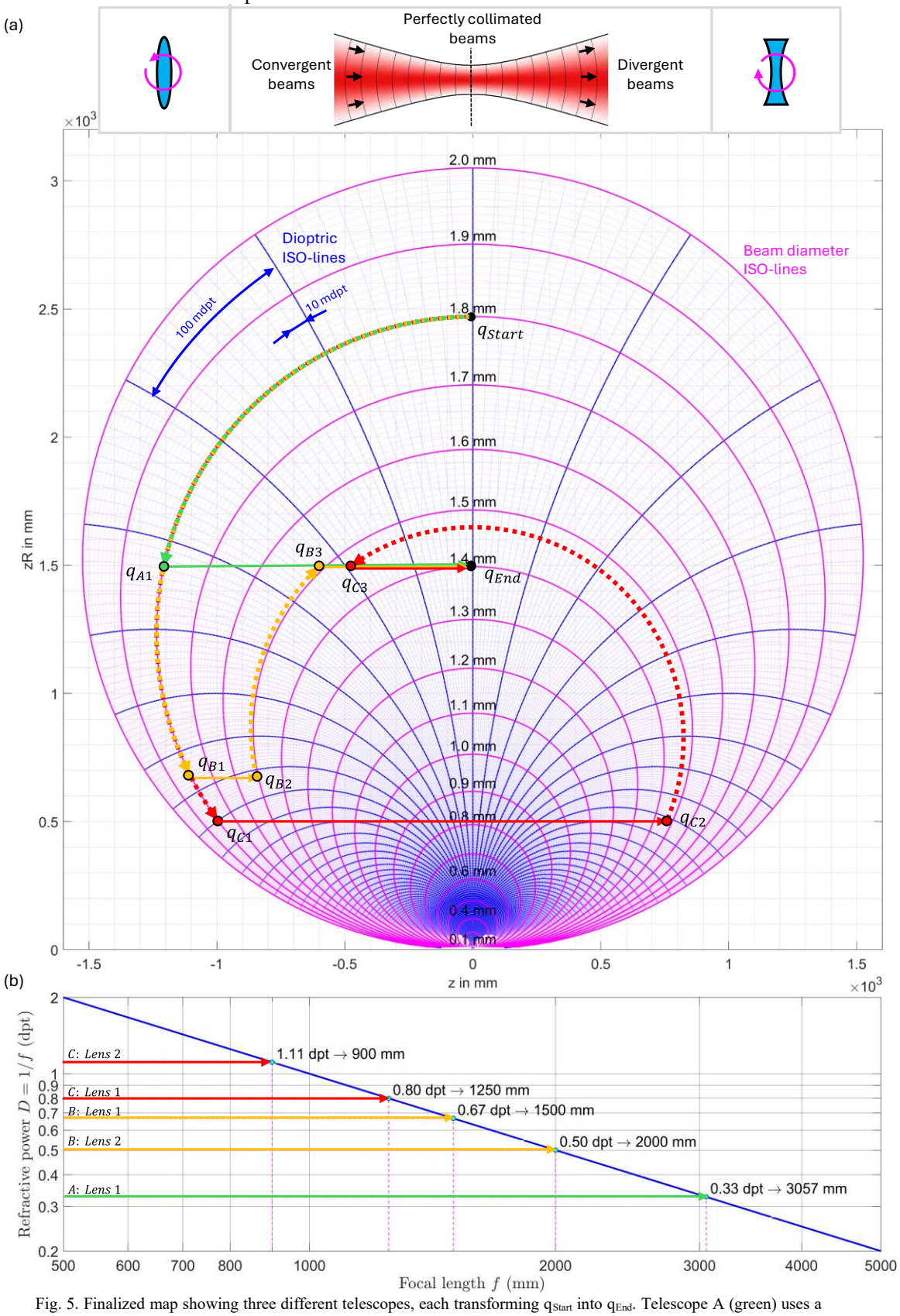


Fig. 5. Finalized map showing three different telescopes, each transforming q_{Start} into q_{End}. Telescope A (green) uses a single lens, telescope B (orange) is a Galilean telescope, and telescope C (red) is a Keplerian telescope. The accompanying graph supports the conversion between dioptric power and focal length. The focal lengths used for the telescopes are highlighted.

To move from q_{Start} to q_{End}, three exemplary telescope configurations are considered. Telescope A uses only one lens. The q-parameter (starting from q_{Start}) must therefore first be moved to the same vertical level, and thus to the same Rayleigh length, as q_{End}. This is achieved with a positive lens, which moves the q-parameter counter-clockwise along the circle on which q_{start} is located. Reaching the Rayleigh length of q_{End} requires the crossing of three major and 2.7 minor dioptric iso-lines, corresponding to 327 mdpt in total. From Fig. 8(b), this corresponds to a focal length of f = 3057 mm. From q_{A1}, the beam then propagates until q_{End} is reached. The propagation distance can be read from the map and is approximately 1200 mm. To prove this method a classic ABCD simulation is shown in Fig. 6.

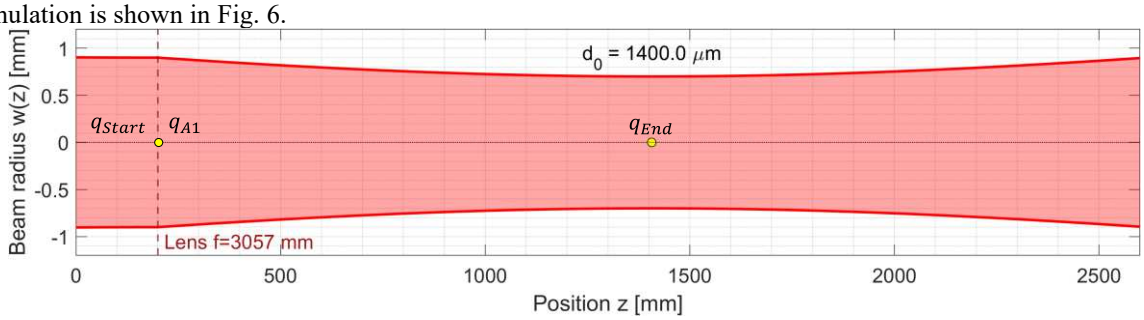


Fig. 6. Simulation of the laser caustic for telescope A from derived from the complex map. The telescope only uses only one lens.

It shows the propagation of the beam through the single-lens telescope from q_{Start} to q_{End}. Note that q_{Start} and q_{A1} coincide in the caustic representation but correspond to different points in the complex map. As in the simulation, the map also indicates the beam diameter during propagation from q_{A1} to q_{End} through the intersections with the magenta iso-diameter rings.

The second example B shows a Galilean telescope. First the beam is focused through a positive lens with a dioptric power of 666 mdpt until reaching q_{B1}. As shown in Fig. 8(b) this dioptric power corresponds to a lens with a focal length of f = 1500 mm. From point q_{B1} on, the beam propagates 253 mm until a second lens is reached (at q_{B2}), having a dioptric power of -500 mdpt, corresponding to a focal length of f = -2000 mm. The distance between the two lenses was chosen such, that q_{B3} is located on the same vertical level (same z_R) as q_{End}. Therefore, only some propagation is needed to meet the required point q_{End}. Fig. 7 shows the corresponding simulation.

Another option would have been to place q_{B2} directly on the same magenta-colored ring (representing the beam diameter) as q_{End} so that no additional propagation would have been required to reach q_{End}. This however would have resulted in a quite unusual focal length, as it was also the case for the lens from telescope A.

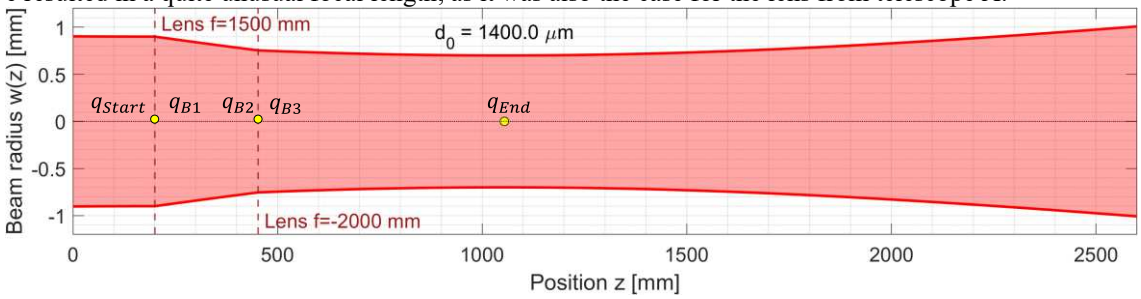


Fig. 7. Simulation of the laser caustic for telescope B from derived from the complex map. The telescope uses a positive and a negative lens in a Galilean setup.

The last telescope C shows a Keplerian telescope. First a very strong lens is used, crossing 8 major dioptric iso-lines on the map, thus amounting to 800 mdpt which corresponds to a lens of f = 1250 mm. After reaching q_{C1}, the beam is propagated through its focus (z = 0 mm) until q_{C2} is reached. At this point a second lens with a dioptric power of 1111 mdpt (f = 900 mm) is implemented, enabling to reach a point q_{C3} which is on the same vertical level (same z_R) as q_{End}. From q_{C3} only a short propagation is required to reach q_{End}. The simulation of this telescope is shown in Fig. 8.

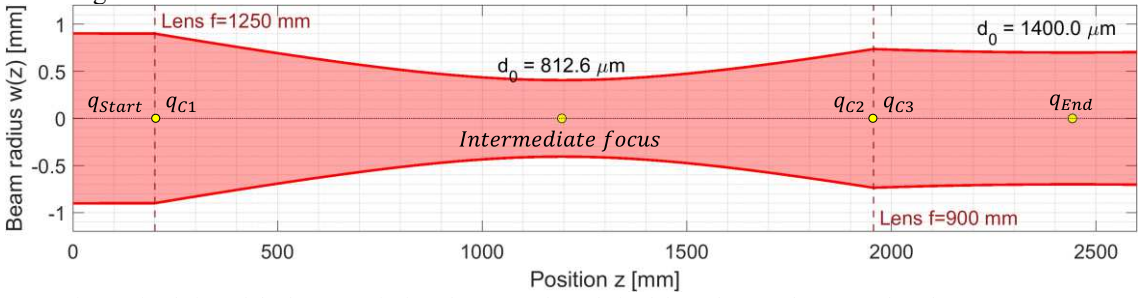


Fig. 8. Simulation of the laser caustic for telescope C from derived from the complex map. The telescope uses two positive lenses in a Keplerian setup.

As these three examples showed, the map is extremely suitable for the designing of telescopes. Compared with a caustic simulation, the map provides several practical advantages. First of all, it is very suitable for comparing the multiple telescope designs, as they can all be displayed within one graph. Furthermore, it shows immediately whether a trajectory reaches the target q-parameter or requires additional propagation. It also makes it straightforward to estimate the influence of tolerances, for example when lens distances are slightly larger or smaller than intended. Also, the required physical lengths of the telescopes can be estimated by comparing the horizontal propagation distances. In addition to this, the beam diameters at the optical elements can easily be assessed from the iso-diameter rings. This is both useful for evaluating LIDT constraints, where larger beam diameters are advantageous, as well as aperture limitations, where the beam must remain sufficiently small. For high-intensity applications, the minimum beam diameter may also be relevant. This can be concluded from the map by evaluating the smallest iso-diameter ring intersected by each beam path.
When designing laser telescopes in practice, the availability of lenses is an additional constraint. For the above shown examples B and C this was considered. For the example A however, where only one lens was allowed, the map clearly showed that no other lens was possible.

7. Conclusion and outlook

This paper presented a graphical method for describing and designing telescopes for Gaussian laser beams using the complex plane and the q-parameter. It was proven analytically that free-space propagation and refraction by thin lenses can be represented by two simple geometrical operations: free-space propagation shifts the q-parameter horizontally, whereas refraction by a lens moves it along a circle defined by the initial q-parameter and the origin of the complex plane. These rules provide an intuitive interpretation of Gaussian beam propagation that complements conventional ABCD-matrix calculations.

Based on these rules, a pre-defined design map was introduced that allows telescope configurations to be developed directly in the complex plane. The map combines q-parameter propagation, dioptric lens power, and information of the beam's diameter in a single graph. As demonstrated for three exemplary telescope layouts, this approach enables rapid comparison of different optical designs, including estimates of propagation distances, lens powers, and beam diameters. The proposed method is particularly useful for early-stage optical design and for laboratory work, where quick and physically intuitive estimates are often required before detailed numerical simulations are performed.
Future work will focus on the implementation of additional optical elements and the development of a simple software tool.

Funding. Ministerium für Wissenschaft, Forschung und Kunst Baden-Württemberg.

Disclosures. The authors declare no conflict of interest

Acknowledgements. The authors would like to thank the Ministry of Science, Research and Arts of the Federal State of Baden-Württemberg for the financial support of the projects within the InnovationsCampus Mobilität der Zukunft.

Data availability. Data underlying the results presented in this paper are not publicly available at this time but may be obtained from the authors upon reasonable request.

References

1. S. S. Lee, H. Ahn, F. De Marco, S. Di, V. Sequino, S. Pak, W. Ali, M. Bawaj, G. Chiarini, B. Garaventa, J. Han, C. Kim, Y. Kim, M. De Laurentis, S. S. Lee, L. Naticchioni, J. Gyu, F. Sorrentino, F. De Marco, S. Di Pace, V. Sequino, S. Pak, W. Ali, M. Bawaj, G. Chiarini, B. Garaventa, J. Han, C. Kim, Y. Kim, M. De Laurentis, S. S. Lee, L. Naticchioni, J. G. Park, and F. Sorrentino, "Design and alignment of a reflective mode matching telescope for squeezing experiments," Opt. Laser Technol. **202**, 115406 (2026).
2. M. Guo, G. Jin, J. Cai, W. Zhang, and Z. Wei, "Study and design of beam expander with wide aperture," in *International Symposium on Optoelectronic Technology and Application 2014: Laser Materials Processing; and Micro/Nano Technologies*, G. Jin, S. Zhuang, and J. Liu, eds. (SPIE, 2014), Vol. 9295, p. 92950T.
3. B. Zhao, W. Zhang, X. Zhou, J. Liu, L. Meng, M. Hu, N. Zhang, A. Chen, W. Zheng, B. I. Z. Hao, W. E. Z. Hang, X. U. Z. Hou, J. I. N. G. L. Iu, L. I. M. Eng, M. H. U. An, N. I. Z. Hang, and A. O. C. Hen, "High beam quality, high brightness dense spectral beam combining of 650 nm laser diode module," Opt. Express **32**, 35840–35853 (2024).
4. T. T. Saha and W. W. Zhang, "Optical design of type-1 x-ray telescopes and their application to STAR-X," Appl. Opt. **61**, 505–516 (2022).
5. C. S. Gardner, B. M. Welsh, L. A. Thompson, C. S. Cardner, L. A. Thompson, and B. M. Welsh, "Design and performance analysis of adaptive optical telescopes using lasing guide stars," Proc. IEEE **78**, 1721–1743 (1990).
6. E. Waluschka and M. V Papalexandris, "LISA Telescope Sensitivity Analysis," **4767**, 114–122 (n.d.).
7. G. Andersen, J. Munch, and P. Veitch, "Holographic correction of large telescope primaries by

proximal, off-axis beacons," Appl. Opt. **35**, 603–608 (1996).
8. W. Shi, R. Li, H. Zhang, C. Liu, X. Zhou, Z. Yuan, Y. Wan, B. He, J. Meng, and X. Hou, "Design of ten-thousand-watt laser beam expander and research on the thermal effect," Opt. Eng. **64**, 75101 (2025).
9. B. E. A. Saleh and M. C. Teich, *Fundamentals of Photonics* (2019).
10. M. Pflüger, V. Soltwisch, J. Probst, F. Scholze, and M. Krumrey, "Grazing-incidence small-angle X-ray scattering (GISAXS) on small periodic targets using large beams.," IUCrJ **4**, 431–438 (2017).
11. G. D. Boyd and H. Kogelnik, "Generalized confocal resonator theory," Bell Syst. Tech. J. **41**, 1347–1369 (1962).
12. F. Bienert, T. Graf, and M. Ahmed Abdou, "Designing of pulse compressors," Opt. Express **Vol. 33**, (2025).
13. T. Li, "Dual Forms of the Gaussian Beam Chart," Appl. Opt. **3**, 1315–1317 (1964).
14. S. A. Collins, "Analysis of Optical Resonators Involving Focusing Elements," Appl. Opt. **3**, 1263–1275 (1964).
15. G. Seifert, "A Logarithmic Gaussian Beam Chart," Appl. Opt. **7**, 337–340 (1968).
16. D. Kessler and R. V Shack, "yy¯ Diagram, a powerful optical design method for laser systems," Appl. Opt. **31**, 2692–2707 (1992).
17. M. Takeda, "New diagram for nomographic design and analysis of paraxial optical systems," J. Opt. Soc. Am. **70**, 236–242 (1980).
18. I. Gere, P. H. A. Sbeck, T. O. W. Uthe, F. R. P. Ichlmeier, V. L. P. Ervak, T. H. K. Inder, H. R. I. Glev, F. R. P. Feiffer, R. E. K. Ienberger, N. Rg̃gere, M. Wurzer, C. Xue, P. Asbeck, T. Wuthe, F. Pichlmeier, V. Pervak, T. Kinder, H. Iglev, F. Pfeiffer, and R. Kienberger, "Mode matching and Pound-Drever-Hall synchronization of a green enhancement cavity with a pulsed Yb:YAG laser," Opt. Express **34**, 30407–30428 (2026).
19. P. Hello and C. N. Man, "Design of a low-loss off-axis beam expander," Appl. Opt. **35**, 2534–2536 (1996).
20. Y. Li, C. Lou, G. Chang, and Y. Gao, "Theoretical study on the actively mode-locked fiber laser with the q-parameter and the ABCD law," IEEE Photonics Technol. Lett. **11**, 1590–1592 (1999).
21. A. M. Kowalevicz, A. Sennaroglu, A. T. Zare, and J. G. Fujimoto, "Design principles of q-preserving multipass-cavity femtosecond lasers," J. Opt. Soc. Am. B **23**, 760–770 (2006).
22. H. Kogelnik and T. Li, "Laser Beams and Resonators," Appl. Opt. **5**, 1550–1567 (1966).
23. A. Sennaroglu and J. G. Fujimoto, "Design criteria for Herriott-type multi-pass cavities for ultrashort pulse lasers," Opt. Express **11**, 1106–1113 (2003).

Appendix A

Within this section it is proven for any q_1 which is transformed by a lens, in the complex plane the resulting q_2 is located on a circle that passes through q_0 and q_1 and whose centre is located on the vertical (imaginary) axis. This means that q_1 is effectively rotated by an angle φ around the point q_M representing the center of the circle.

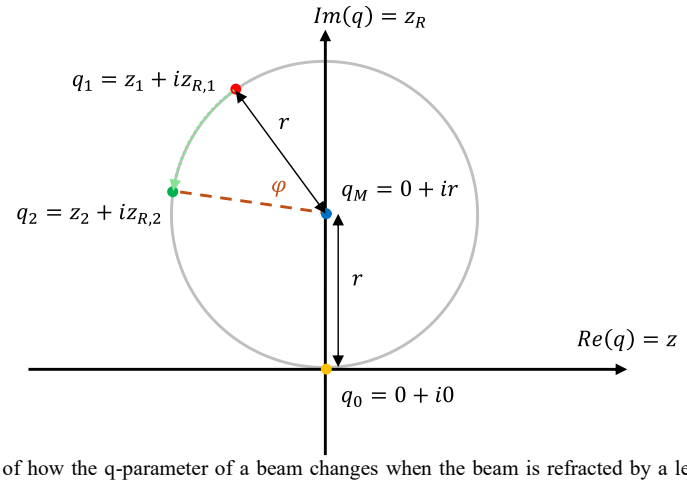


Fig. 9. Illustration of how the q-parameter of a beam changes when the beam is refracted by a lens. The original q-parameter q_1 (before the lens) is mathematically rotated around a point q_M by an angle φ. The point q_M is located on the vertical axis (with $z = 0$) which has the same distance to q_1 and q_0. The angle φ depends both on the q-parameter q_1 and the focal length of the lens.

Derivation of the circle's radius r

First, the radius r of the circle is derived. The initial q-parameter q_1 is given by

$$q_1 = z_1 + iz_{R,1}. \tag{10}$$

The point q_M is defined as the center of the circle, while both q_1 and q_0 lie on its circumference. It therefore follows that

$$|q_1 - q_M| = |q_M - q_0| \tag{11}$$

Implementing q_1, q_M with

$$q_M = ir \tag{12}$$

and q_0 with

$$q_0 = 0 \tag{13}$$

as defined by Fig. 3 into Eqn. (11) leads to

$$\left|z_1 + iz_{R,1} - ir\right| = |ir - 0|. \tag{14}$$

This simplifies to

$$\left|z_1 + i\left(z_{R,1} - r\right)\right| = r. \tag{15}$$

Using the Pythagorean theorem, it can be transformed into

$$\sqrt{z_1^2 + \left(z_{R,1} - r\right)^2} = r \tag{16}$$

and

$$z_1^2 + \left(z_{R,1} - r\right)^2 = r^2. \tag{17}$$

Expanding the expression gives

$$z_1^2 + z_{R,1}^2 - 2z_{R,1}r + r^2 = r^2 \tag{18}$$

Finally, r is obtained as

$$r = \frac{z_1^2 + z_{R,1}^2}{2z_{R,1}} \tag{19}$$

Derivation of the distance between q_2 and q_M

Starting with q_1 defined as

$$q_1 = z_1 + iz_{R,1} \tag{20}$$

and using the transformation equation

$$q_2 = \frac{A \cdot q_1 + B}{C \cdot q_1 + D} \tag{21}$$

together with the matrix of a thin lens,

$$M_{Lens} = \begin{bmatrix} A & B \\ C & D \end{bmatrix} = \begin{bmatrix} 1 & 0 \\ C & 1 \end{bmatrix} \tag{22}$$

q_2 is obtained as

$$q_2 = \frac{q_1}{Cq_1 + 1}. \tag{23}$$

The distance d between q_2 and q_M is given by

$$d = |q_2 - q_M|. \tag{24}$$

Squaring this expression leads to

$$d^2 = |q_2 - q_M|^2. \tag{25}$$

Replacing q_M with Eqn. (12), replacing q_2 with Eqn. (23) and simplifying the expression leads to

$$d^2 = |q_2 - ir|^2 = \left|\frac{q_1}{Cq_1 + 1} - ir\right|^2 = \left|\frac{q_1 - ir(Cq_1 + 1)}{Cq_1 + 1}\right|^2. \tag{26}$$

This expression can be written as

$$d^2 = \frac{|q_1 - irCq_1 - ir|^2}{|Cq_1 + 1|^2}. \tag{27}$$

To simply this equation we first simplify the numerator of this equation, using its complex conjugate as

$$|q_1 - irCq_1 - ir|^2 = (q_1 - irCq_1 - ir) \cdot (\overline{q_1 - irCq_1 - ir}) \tag{28}$$

This further simplifies to

$$|q_1 - irCq_1 - ir|^2 = (q_1 - irCq_1 - ir) \cdot (\bar{q_1} - irC\bar{q_1} - ir). \tag{29}$$

Using Eqn. (19) for r, together with the identity

$$z_1^2 + z_{R,1}^2 = q_1\bar{q_1} \tag{30}$$

we find

$$r = \frac{q_1\bar{q_1}}{2z_{R,1}}. \tag{31}$$

Substituting this result into Eq. (29) gives

$$|q_1 - irCq_1 + ir|^2 = q_1\bar{q_1} \cdot (1 + C^2r^2) - 2r \cdot z_{R,1} + 2Cr^2 \cdot z_1 + r^2 \tag{32}$$

Rearranging Eqn. (31) as

$$-2r \cdot z_{R,1} = q_1\bar{q_1} \tag{33}$$

and implementing it into Eqn. (32) yields

$$|q_1 - irCq_1 + ir|^2 = q_1\bar{q_1} + q_1\bar{q_1} \cdot C^2r^2 - q_1\bar{q_1} + 2Cr^2z_1 + r^2. \tag{34}$$

This simplifies to

$$|q_1 - irCq_1 + ir|^2 = q_1\bar{q_1} \cdot C^2r^2 + 2Cr^2z_1 + r^2 \tag{35}$$

and finally, to

$$|q_1 - irCq_1 + ir|^2 = r^2(q_1\bar{q_1} \cdot C^2 + 2Cz_1 + 1). \tag{36}$$

To simplify the denominator of Eqn. (27), the complex conjugate is used as

$$|Cq_1 + 1|^2 = (Cq_1 + 1) \cdot (C\bar{q_1} + 1). \tag{37}$$

Expanding this expression results in

$$|Cq_1 + 1|^2 = q_1\bar{q_1} \cdot C^2 + 2Cz_1 + 1. \tag{38}$$

Implementing both the numerator (Eqn.(36)) and the denominator (Eqn. (38)) back into Eqn. (27) finally results in

$$d^2 = |q_2 - q_M|^2 = \frac{r^2(q_1\bar{q_1} \cdot C^2 + 2Cz_1 + 1)}{q_1\bar{q_1} \cdot C^2 + 2Cz_1 + 1} = r^2. \tag{39}$$

From this

$$d = r \tag{40}$$

can be followed, proving that q_2 always lies on the above-defined circle as independent of the value C.

Appendix B

Within this section the angle of rotation φ between q_1 and q_2 (around the point q_M) is derived, cf. Fig. 4. (a). To begin with, q_M is subtracted from both q_1 and q_2, effectively moving them to the center of the complex plane, see Fig. 4. (b).

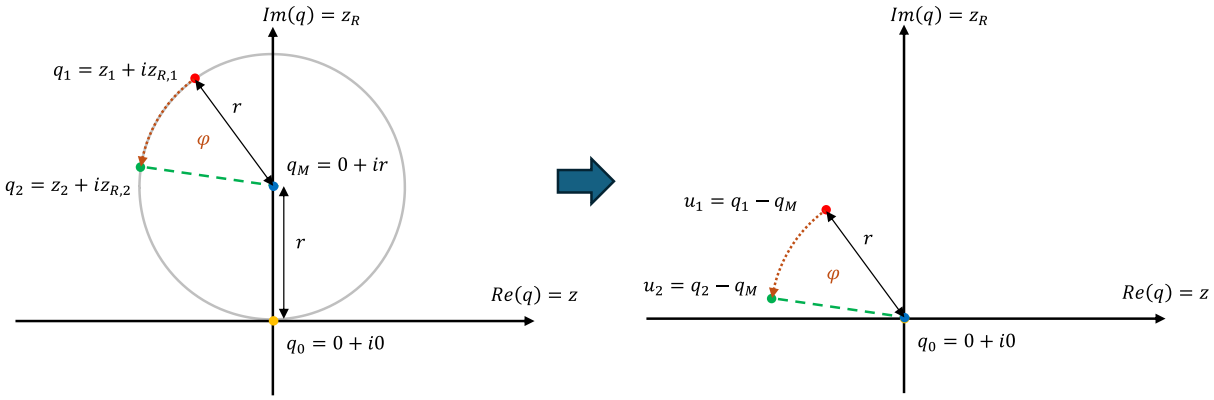


Fig. 4. (a): Relations among q_1, q_2, q_M, and q_0. To determine the rotation angle φ, q_M is subtracted from q_1 and q_2. (b): This translation moves the center of the circle to the origin and defines the translated complex numbers u_1 and u_2.

Therefore, the new complex numbers u_1 and u_2 are created being defined as

$$u_1 = q_1 - q_M = r_1 \cdot e^{\theta_1} \tag{41}$$

and

$$u_2 = q_2 - q_M = r_2 \cdot e^{\theta_2}, \tag{42}$$

respectively. In order to determine the angle between them u_2 is divided by u_1 creating a new complex number v, defined as

$$v = \frac{u_2}{u_1} = \frac{r_2 \cdot e^{\theta_2}}{r_1 \cdot e^{\theta_1}}. \tag{43}$$

with r_1 being identical to r_2, v incorporated the angle φ as

$$v = \frac{u_2}{u_1} = 1 \cdot e^{\theta_2 - \theta_1} = e^{\varphi}. \tag{44}$$

By implementing Eqn. (41), Eqn. (42) and Eqn. (23) v can be written as

$$v = \frac{u_2}{u_1} = \frac{q_2 - q_M}{q_1 - q_M} = \frac{\frac{q_1}{Cq_1 + 1} - ir}{q_1 - ir}. \tag{45}$$

This simplifies to

$$v = \frac{q_1 - ir(Cq_1 + 1)}{(Cq_1 + 1)(q_1 - ir)} = \frac{q_1 - ir - irCq_1}{(Cq_1 + 1)(q_1 - ir)}. \tag{46}$$

By multiplying it with the complex conjugate of one term from the denominator v is given as

$$v = \frac{(q_1 - ir - irCq_1)(\bar{q}_1 + ir)}{(Cq_1 + 1)(q_1 - ir)(\bar{q}_1 + ir)}. \tag{47}$$

From Eqn. (12) and Eqn. (24) u_1 can be defined as

$$u_1 = q_1 - ir. \tag{48}$$

From that it is found that

$$(q_1 - ir)(\bar{q}_1 + ir) = u_1 \cdot \bar{u}_1 = r^2. \tag{49}$$

Implementing this into Eqn. (47) results in

$$v = \frac{(q_1 - ir - irCq_1)(\bar{q}_1 + ir)}{(Cq_1 + 1)r^2} \tag{50}$$

Simplifying the numerator with Eqn. (30) and Eqn. (31) v can be written as

$$v = \frac{r^2\left((1 + Cz_1) - iCz_{R,1}\right)}{(Cq_1 + 1)r^2} = \frac{(1 + Cz_1) - iCz_{R,1}}{(Cq_1 + 1)} \tag{51}$$

After splitting up q_1 in the numerator v is given as

$$v = \frac{(1 + Cz_1) - iCz_{R,1}}{(1 + Cz_1) + iCz_{R,1}}. \tag{52}$$

To separate the real and the imaginary part the equation is multiplied with the complex conjugate of the denominator, resulting in

$$v = \frac{(1 + Cz_1) - iCz_{R,1}}{(1 + Cz_1) + iCz_{R,1}} \cdot \frac{(1 + Cz_1) - iCz_{R,1}}{(1 + Cz_1) - iCz_{R,1}} \tag{53}$$

and

$$v = \frac{(1 + Cz_1)^2 - 2iCz_{R,1}(1 + Cz_1) - \left(Cz_{R,1}\right)^2}{(1 + Cz_1)^2 + \left(Cz_{R,1}\right)^2} \tag{54}$$

and finally

$$v = \frac{(1 + Cz_1)^2 - \left(Cz_{R,1}\right)^2}{(1 + Cz_1)^2 + \left(Cz_{R,1}\right)^2} + i\frac{-2iCz_{R,1}(1 + Cz_1)}{(1 + Cz_1)^2 + \left(Cz_{R,1}\right)^2} \tag{55}$$

Although v is now formulated in such a form that the angle φ could be directly determined as the argument of v as

$$\varphi = \operatorname{atan}\left(\frac{Im(v)}{Re(v)}\right) \tag{56}$$

such approaches typically run into the common issues associated with errors $\pm k \cdot \pi$, depending on the quadrant v is located in. To avoid using atan2 as a computational solution, the so-called half-angle approach is followed. Using the half-angle approach, an auxiliary complex number v_{half} is chosen such that its argument is half the argument of v, i.e.

$$\arg\left(v_{half}\right) = \theta = \frac{\varphi}{2} \tag{57}$$

Since the principal value of φ is taken in the interval (−π,π), the corresponding half-angle θ lies in the interval (−π/2,π/2), i.e. in the first of fourth quadrant, as schematically shown in Fig. 5. In this interval, the tangent function is single-valued, so θ can be determined unambiguously using the arctangent. The desired rotation angle is then obtained by doubling the half-angle, i.e. φ = 2θ. This procedure avoids the quadrant ambiguity that occurs when the argument of v is calculated directly from a simple arctangent and is illustrated schematically in Fig. 5.

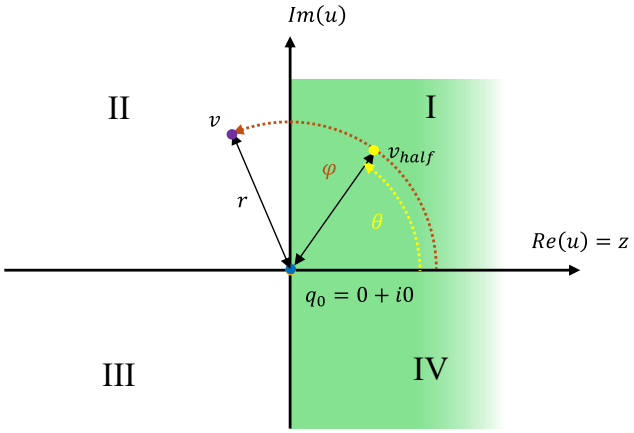


Fig. 5. (a): Schematic illustration showing how the half-angle approach works. Instead of determining the angle φ the angle θ (which is exactly half of φ) is determined using the arctan-function. By doing this, it is ensured that θ is always located either in the first or in the fourth quadrant, where the interval of the arctan is valid.

To start with, v is defined via a new complex number v_{half} such that is has the same radius but the discussed halved angle θ. Therefore, v can be defined as

$$v = \frac{v_{half}^2}{|v|^2} \tag{58}$$

since

$$v = \frac{v_{half}^2}{|v|^2} = \frac{r \cdot e^{i\theta} \cdot r \cdot e^{i\theta}}{r^2} = r \cdot e^{i2\theta} = r \cdot e^{i\varphi}. \tag{59}$$

Using the algebraic form of v_{half}, v can be stated as

$$v = \frac{(a+bi)^2}{|v|^2} = \frac{a^2 + 2abi - b^2}{|v|^2} = \frac{a^2 - b^2}{|v|^2} + \frac{2abi}{|v|^2}. \tag{60}$$

Since

$$|v|^2 = \left|v_{half}\right|^2 = a^2 + b^2 \tag{61}$$

Eqn. (60) can also be formulated as

$$v = \frac{a^2 - b^2}{a^2 + b^2} + \frac{2abi}{a^2 + b^2}. \tag{62}$$

At the same time, from Eqn. (56) it can be followed that

$$\varphi = 2 \cdot \theta = 2 \cdot \arctan\left(\frac{Im(v_{half})}{Re(v_{half})}\right) = 2 \cdot \arctan\left(\frac{b}{a}\right). \tag{63}$$

Now the final trick comes into play. One the one hand, v is defined as

$$v = \frac{a^2 - b^2}{a^2 + b^2} + \frac{2abi}{a^2 + b^2} \tag{64}$$

And on the other hand, it is defined as

$$v = \frac{(1 + Cz_1)^2 - \left(Cz_{R,1}\right)^2}{(1 + Cz_1)^2 + \left(Cz_{R,1}\right)^2} + i\frac{-2iCz_{R,1}(1 + Cz_1)}{(1 + Cz_1)^2 + \left(Cz_{R,1}\right)^2}. \tag{65}$$

Comparing these terms, it can easily be seen that either

$$a = (1 + Cz_1) \tag{66}$$

and

$$b = -Cz_{R,1} \tag{67}$$

or that

$$a = -(1 + Cz_1) \tag{68}$$

and

$$b = C z_{R,1}. \tag{69}$$

For the angle φ however, it doesn't matter whether a or b is defined negative and from Eqn. (63) φ can now finally be defined as

$$\varphi = 2 \cdot \arctan\left(-\frac{C z_{R,1}}{1 + C z_1}\right). \tag{70}$$

By applying additional modification this expression can be transformed into

$$\varphi = -2 \cdot \arctan\left(\frac{z_{R,1}}{\frac{1}{C} + z_1}\right) \tag{71}$$

and

$$\varphi = -2 \cdot \arctan\left(\frac{z_{R,1}}{z_1 - f}\right). \tag{72}$$